Angewandte Corrigendum

Efficient Homogeneous Electrocatalytic Water Oxidation by a Manganese Cluster with Overpotential of Only 74 mV

Angew. Chem. Int. Ed. **2019**, *58*

DOI: 10.1002/anie.201813895

The authors of this Communication request that George Christou be inserted as an additional author. The author list should read as follows:

Totan Ghosh, George Christou, and Galia Maayan*

The affiliation for George Christou is:

Prof. G. Christou, Department of Chemistry, University of Florida, Gainesville, FL (USA)

All authors of the original manuscript have agreed with the addition of G. Christou as a co-author.

Electrochemistry

Deutsche Ausgabe: DOI: 10.1002/ange.201813895
Internationale Ausgabe: DOI: 10.1002/anie.201813895

Efficient Homogeneous Electrocatalytic Water Oxidation by a Manganese Cluster with an Overpotential of Only 74 mV

*Totan Ghosh and Galia Maayan**

Abstract: *Water electrolysis is among the simplest method for generating hydrogen as an alternative renewable fuel. A major challenge associated with this process is the development of cheap, simple, and environmentally benign catalysts that lead to a minimum overpotential for water oxidation. Inspired by the Mn_4CaO_x cluster that catalyzes water oxidation in photosystem II, described here is the synthesis and characterization of the manganese cluster $[Mn_{12}O_{12}(O_2CC_6H_2(OH)_3)_{16}(H_2O)_4]$ ($Mn_{12}TH$) along with its electrocatalytic activity at pH 6. Electrochemical, spectroscopic, and electron microscopy studies show that $Mn_{12}TH$ is a homogeneous electrocatalyst for water oxidation and enables oxygen evolution with a reaction rate of 22 s^{-1}, high Faradic efficiency (93 %), and an overpotential of only 74 mV, the lowest reported to date. Based on the electrochemical data, the organic ligands, which can be described as the second coordination sphere of the catalytic manganese core, play a key role in facilitating the oxidation process and accelerating the reaction.*

One of the promising approaches for clean fuel generation is water splitting to produce molecular oxygen and hydrogen, the latter being a renewable energy source.[1] The production of molecular hydrogen from water involves two half reactions: 1) water oxidation: $2H_2O = O_2 + 4H^+ + 4e^-$ and 2) proton reduction: $2H^+ + 2e^- = H_2$. From these two, water oxidation (WO) is the bottleneck of the whole water splitting process because of the transfer of multiple protons and electrons and the very high thermodynamic potential required for this reaction [$E^0 = 1.23$ V vs. normal hydrogen electrode (NHE), $E_{pH\,6} = 0.876$ V vs. NHE].[2] Over the years, many heterogeneous WO catalysts have been developed.[3] Compared to heterogeneous catalysts, homogeneous systems enable rational design of molecular catalysts, facilitate understanding of reaction mechanism, and can be systematically tuned and optimized. Given these advantages, several transition-metal complexes have been developed as homogeneous catalysts for WO and are based on the metal ions Ru,[4] Ir,[5] Fe,[6] Co,[7] Cu,[8] and Mn.[9] Further advances require the development of catalysts that are not only based on earth-abundant metals, but are also stable, fast and, most importantly, can perform with as low overpotential as possible to meet practical applications. One approach to address these goals is to mimic the structure and function of the oxygen-evolving complex (OEC) in photosystem II (PSII), which is a manganese-oxo cluster. Although various structural mimics of the OEC are reported,[10] manganese-based homogeneous water oxidation electrocatalysts are very scant.[11] Recently, our group reported the water-soluble manganese-based electrocatalyst $[Mn_{12}O_{12}(O_2CC_6H_3(OH)_2)_{16}(H_2O)_4]$ ($Mn_{12}DH$),[12] which structurally mimics the OEC and operates at pH 6 with a low overpotential of only 334 mV, average k_{obs} of 0.035 s^{-1} (based on Foot-of-the-wave analysis, FOWA), and Faradic efficiency (FE) of 80 % (see Table T1 in the Supporting Information). We suggested that the hydroxy groups on the organic ligands, which can be described as the second coordination sphere of the manganese catalyst, may contribute to the catalysis by either proton transfer or shuttling and/or by facilitating the formation of high-valence species required for water oxidation. To probe the role of the hydroxy substituent in the electrocatalytic activity, aiming to increase the rate and efficiency of the reaction and to lower its overpotential even further, we are currently developing similar manganese clusters from different organic ligands.

Herein we describe the successful synthesis of a new cluster, $[Mn_{12}O_{12}(O_2CC_6H_2(OH)_3)_{16}(H_2O)_4]$ ($Mn_{12}TH$, Figure 1 a), which is based on the ligand 3,4,5-trihydroxy benzoic acid (thbH), and its electrocatalytic WO activity. We have discovered that this small change in the second coordination sphere about the metal center leads to almost three orders of magnitude faster ($k_{obs} = 22$ s^{-1}) and highly efficient (93 % FE) catalytic water oxidation activity at pH 6 with an overpotential of only 74 mV. This value is the lowest overpotential reported for homogeneous a WO electrocatalyst by any first-row transition-metal complex to date (see Table T2). Based

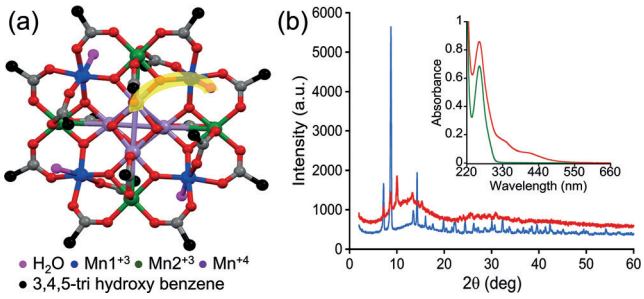

Figure 1. a) Suggested structure of $[Mn_{12}O_{12}(O_2CC_6H_2(OH)_3)_{16}(H_2O)_4]$ ($Mn_{12}TH$) viewed along the molecular *x* axis. The Mn^{4+}-*O*-$Mn1^{3+}$-H_2O motif is highlighted in yellow. Hydrogen atoms are omitted for clarity. The structure was adapted from Ref. [13]. b) Powder XRD pattern of the cluster $Mn_{12}TH$ (red line) and $Mn_{12}Ac$ (blue line). Inset: UV/Vis spectrum of the complex $Mn_{12}TH$ (red line) and thbH ligand (green line).

[*] Dr. T. Ghosh, Prof. G. Maayan
Schulich Faculty of Chemistry, Technion-Israel Institute of Technology
Technion City, Haifa 3200008 (Israel)
E-mail: gm92@technion.ac.il
Supporting information and the ORCID identification number(s) for the author(s) of this article can be found under: https://doi.org/10.1002/anie.201813895.

on the pH-dependent redox properties of thbH and $Mn_{12}TH$, and on our electrochemical data, we propose the first two steps of the reaction with $Mn_{12}TH$ and suggest that the oxidation of the additional OH group by the applied potential assists in stabilizing the higher oxidation state of the catalytic manganese ion, thus enhancing the reaction rate and lowering the overpotential.

The highly water-soluble $Mn_{12}TH$ cluster was prepared in aqueous medium by adopting, with some modifications, the synthetic procedure used for the synthesis of $[Mn_{12}O_{12}(O_2CCH_3)_{16}(H_2O)_4]$ ($Mn_{12}Ac$)[14]. The full synthesis is described in the Supporting Information. $Mn_{12}TH$ was characterized by a collection of different analytical methods. The IR spectrum showed some distinct peaks in the range of $\upsilon = 610$–$720\ cm^{-1}$ corresponding to the various Mn–O stretching modes and at $\upsilon = 1023$, $1041\ cm^{-1}$ for the Ar-O-H stretching frequencies.[15] This spectrum was further compared to the IR spectrum of $[Mn_{12}O_{12}(O_2CC_6H_5)_{16}(H_2O)_4]$ ($Mn_{12}Bz$), which we synthesized according to a literature method.[14] The high similarity between the two spectra, specifically in the region of the carboxylate bands ($\upsilon = 2000$–$1000\ cm^{-1}$), suggests that $Mn_{12}TH$ retains the $[Mn_{12}O_{12}(O_2CR)_{16}(H_2O)_4]$ structure (see Figure S2). This structure was further supported by powder XRD analysis showing diffraction peaks at 2θ values of 7.17, 8.96, 10.06, and 13.66, consistent with the reported powder XRD pattern of Mn_{12} stearate[16] and of pure crystals of $Mn_{12}Ac$ synthesized in our lab (Figure 1b). Additionally, the ESI-MS analysis of $Mn_{12}TH$ in water showed a peak at 3627.1 (cal. Mw = 3627.46) corresponding to the full mass of the cluster (see Figure S3). Furthermore, the UV/Vis spectrum of $Mn_{12}TH$ showed an absorption band near $\lambda_{max} = 260$ nm corresponding to the π–π* transition of thbH and two broad bands near $\lambda = 335$ nm and 420 nm, which arise from the ligand-to-metal charge-transfer transition and metal d–d transition, respectively (Figure 1b, inset). Experimental data from a C, H, N analysis indicated the presence of 20 water molecules outside the cluster moiety. Thermogravimetric analysis supported these results, showing that 9.6% weight loss is taking place in the temperature range between 90°C and 150°C (see Figure S4), and is in agreement with the calculated weight loss (9.03%) for 20 water molecules. Collectively, the experimental analysis provides strong evidence for the formation of the $Mn_{12}TH$ structure as shown in Figure 1a.

Cyclic voltamograms (CVs) of thbH and $Mn_{12}TH$ were performed in aqueous acetate buffer at pH 6.0, the pH at which the OEC within PSII shows optimal catalytic performance,[17] and at which $Mn_{12}TH$ was found to be stable for a long time. The CV of thbH shows two oxidation waves at 0.7 V and 0.95 V vs. NHE (Figure 2a, black line). These waves are attributed to the oxidation of the *para* OH group (*para*OH) to form a semiquinone radical, followed by the oxidation of a *meta* OH group to form a quinone, respectively (see Scheme S1).[18] Both processes involve one proton and one electron oxidation each, with no peaks on the reverse scan, indicating that this process is irreversible, as previously demonstrated.[18,19] We note here, that the pH-dependence study of thbH is also well described in the literature, showing that the peak potential shifts to a lower potential region as the

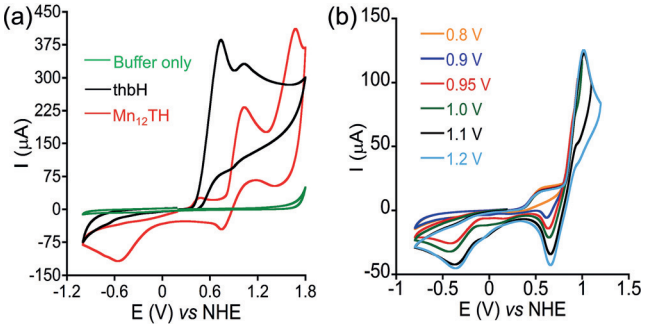

Figure 2. a) CV scans of a 0.1 M acetate buffer at pH 6 (green line), with 0.5 mM thbH (black line) and with 0.5 mM $Mn_{12}TH$ (red line) using a glassy carbon electrode ($S = 0.07\ cm^2$). b) CV scans of $Mn_{12}TH$ in 0.1 M acetate buffer pH 6 taken at different potential ranges.

pH is increased from 2 to 7, indicating that the electrode process is influenced by the protonation reactions.[18] The CV of $Mn_{12}TH$ at pH 6, scanning in the anodic direction, shows three oxidation waves at $E_p = 0.5$, 1.0, and 1.67 V vs. NHE and two reduction peaks at $E_p = 0.75$ and −0.5 V vs. NHE (Figure 2a, red line). The first oxidation wave is assigned to the oxidation of the *para*OH, the second and third waves at 1.0 V and 1.67 V, respectively, can be each assigned to the oxidation of one Mn^{+3} to Mn^{+4}.[14b] As the carboxylate group of thb^- is bonded to the manganese ion(s), the oxidation of the *para*OH is further facilitated and hence takes place at lower potential compared to the same oxidation within thbH (0.5 vs. 0.7 V). The absence of a corresponding reduction peak suggests that the oxidation of *para*OH within $Mn_{12}TH$ is also irreversible. The pH-dependent reduction peak at 0.75 V could be assigned to the reduction of Mn^{+4}=O to Mn^{+3}-OH. The new reduction peak at −0.5 V could be assigned to the reduction of produced O_2 to O_2^-,[12] suggesting that the oxidation of $Mn_{12}TH$ triggers electrocatalytic WO to O_2. To verify that the reduction peak at −0.5 V corresponds to the O_2/O_2^- reduction, we reversed the CV scan direction after purging the solution with argon gas and scanned first in the cathodic direction from 0 to −1.0 V and then continued to the anodic direction until 1.7 V vs. Ag/AgCl. This CV experiment showed that the −0.5 V feature was absent in the first cycle but appeared again in the following cycle, indicating that it arises from the high-potential oxidation process, in which oxygen is being produced (see Figure S5).[8a,12]

The pH-dependent CV study performed with $Mn_{12}TH$ at pH 4–7 showed that the intensity and oxidation potential of the wave at 1.0 V at pH 6 and 7 are very similar. When decreasing the pH to 5 and then to 4, this oxidation wave shifts towards higher potential and its intensity decreases significantly at pH 4 (see Figure S6a). The slope of $129\ mV\ pH^{-1}$ obtained from plotting the E (V) against the pH suggests that the oxidation at 0.95 V takes place by a loss of two protons (see Figure S6b).[18,19]

To find out the minimum potential at which evolution of oxygen occurs, we performed CV experiments with $Mn_{12}TH$, scanning at $100\ mV\ s^{-1}$ from 0 to 0.8 (which is the onset potential for the oxidation of the first Mn^{3+} to Mn^{4+}), 0.9, 0.95, 1, 1.1 and 1.2 V vs. NHE (Figure 2b). The CV data showed that oxygen evolution takes place already at a potential as low

as 0.95 V vs. NHE, by the appearance of the wave at −0.45 V vs. NHE, which corresponds to the O_2/O_2^- couple.[12] The shift in reduction potential from −0.5 to −0.45 V suggests that the oxidation process is diffusion controlled.

Controlled potential electrolysis (CPE) was therefore performed at 0.75 V vs. Ag/AgCl (0.95 V vs. NHE) to quantify the total evolved oxygen. Evolution of molecular oxygen was investigated by a 5 hour CPE experiment with a porous glassy carbon working electrode in 0.1 M acetate buffer solution, at pH 6, containing 5 mL of 0.5 mM Mn_{12}TH. This electrolysis experiment afforded a total of 157 μM of oxygen, which is 32.5 μmole in 5 hours of electrolysis in 0.1 M acetate buffer at pH 6 (Figure 3a). The total accumulated

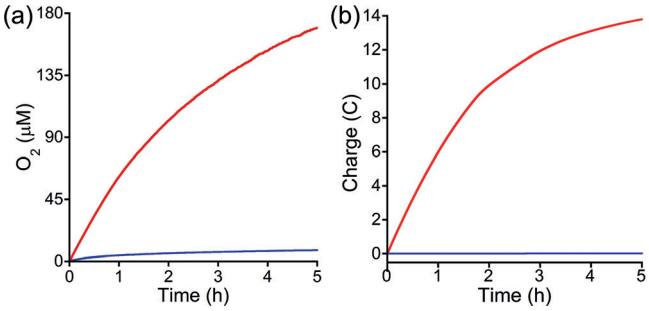

Figure 3. a) Evolution of O_2 measured with a fluorescence probe and b) Total accumulated charge during CPE, both from a solution containing 0.5 mM Mn_{12}TH (red lines), and the buffer only (blue lines), using a porous carbon working electrode at 0.95 V vs. NHE. All solutions contained 0.1 M acetate buffer at pH 6.

charge during this process was 13.8 C (Figure 3b). Based on a 4 e^- process and initial amount of catalyst in solution, the FE and the catalytic TON were calculated to be 93% and 13.2 in 5 hours, respectively (see details in the Supporting Information). The pH of the solution measured at the end of the reaction was 4.9, consistent with the production of protons during electrocatalytic WO.[8b,c] The overpotential for this catalytic process was only 74 mV, the lowest in homogeneous electrocatalytic WO reactions reported to date (see Table T2).

To investigate whether the catalytic process is truly homogeneous, we performed a CV scan in acetate buffer at pH 6 in the absence of Mn_{12}TH, added the cluster, and performed 25 continuous CV scans, and then took out the electrode and rinsed it with water without polishing it. This electrode was then placed in an acetate buffer solution at pH 6 that did not contain Mn_{12}TH, and another CV scan was performed (see Figure S8,S9). This scan was almost identical to the first one taken in the absence of the cluster, suggesting no deposition of the catalyst on the electrode surface. Moreover, the CV scan of the first cycle is also almost identical to that of the 25th cycle, with the only difference being the wave at 0.5 V, which is missing in the 25th cycle because of the irreversible oxidation of thb^-. Additionally, we performed another rinse test, according to Artero et al.,[20] in which we took out the glassy carbon electrode after 25 continuous CV scans, dried it in air without rinsing or polishing its surface, dipped it in 0.1 M acetate buffer solution at pH 6, and ran another CV scan. The obtained voltamogram (blue line, Figure 4a) was also almost identical to this of the blank buffer solution (green line, Figure 4a). Overall, these CV measurements suggest that there is no deposition of any

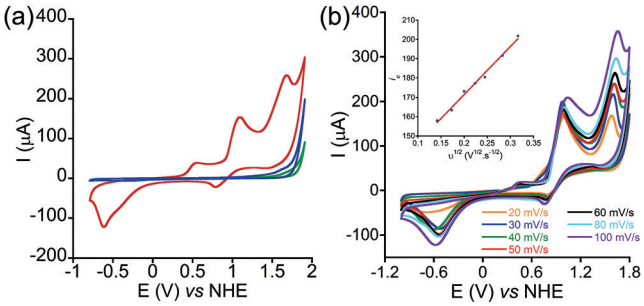

Figure 4. a) CVs of 0.1 M acetate buffer solution at pH 6 in the absence of Mn_{12}TH (green), in the presence of Mn_{12}TH (red), and in the absence of Mn_{12}TH but with the electrode used for 25 scans in the presence of Mn_{12}TH, which was neither rinsed nor polished (blue). b) CVs of a 0.5 mM Mn_{12}TH in different scan rates using a glassy carbon electrode ($S = 0.07$ cm^2, pH 6, 0.1 M acetate buffer). Inset: a plot of the catalytic peak current (i_c) vs. the square root of the scan rate ($R = 0.99$).

particle on the working electrode surface and that Mn_{12}TH is a stable catalyst in solution. To support this conclusion, SEM analysis of the working glassy carbon electrode, before and after the 25 scans, was performed and further confirmed that no particles were adsorbed on the electrode surface (see Figure S10). HRSEM analysis of the glassy carbon electrode before (see Figure S11) and after 5 h of a control potential electrolysis (see Figure S12) also showed that there is no deposition of any particle on the electrode surface. In addition, DLS analyses of the Mn_{12}TH cluster before and after 5 hours of electrolysis in 0.1 M acetate buffer solution (see Figure S13) showed that the particle distribution is in the range of 0.9–1.5 nm, which is the molecular hydrodynamic diameter of the cluster only, indicating that there is no formation of new particles taking place during electrolysis. Collectively, these experiments strongly suggest that Mn_{12}TH is a truly homogeneous WO electrocatalyst.

Additionally, CVs were recorded at different scan rates (Figure 4b) to verify that the catalytic process is diffusion controlled (thus homogeneous). We examined the scan rate dependence oxidation currents at −0.5 V, 1.0 V, and 1.67 V vs. NHE respectively in 0.1 M acetate buffers at pH 6 and obtained a linear fit when the intensity at the peak of each oxidation event was plotted against the square root of the scan rate (Figure 4b, see Figures S14 and S15). These results indicate that the oxidation currents are diffusion controlled and the catalytic process is truly homogeneous.

To find out the k_{obs} value of this catalytic reaction we followed a methodology that was developed by Saveant et al. for electrocatalytic processes, known as foot-of-the-wave analysis (FOWA).[21] Considering no side-phenomenon perturbs the catalytic reaction (at the very beginning of it), the reaction is fast as compared to Fv/RT, in which v is the scan rate, thus it is independent of scan rate and can be described by the following equation:

$$\frac{i}{FS} = \frac{Cp^0\sqrt{Dp2kC_A^0}}{1+\exp\left[\frac{F}{RT}(E-E^0)\right]} \quad (1)$$

The peak current of the catalyst in the absence of substrate[22] may serve to calibrate the catalytic response in terms of electrode surface area, S, catalyst concentration, C_p^0, diffusion coefficient, D_p, and scan rate, ν.

$$\frac{i_p^0}{FS} = 0.446Cp^0\sqrt{Dp.}\sqrt{\frac{Fv}{RT}} \quad (2)$$

It is thus convenient to observe the variation of i/i_p^0 as:

$$\frac{i}{i_p^0} = \frac{2.24\sqrt{\frac{RT}{Fv}2kC_A^0}}{1+\exp\left[\frac{F}{RT}(E-E^0)\right]} \quad (3)$$

Here i_c, catalytic peak current at 0.95 V; i_d, non- catalytic peak current at 0.75 V; $E^0 = 0.95$ V, $k =$ catalytic rate constant $= k_{obs.}$

Plotting i_c/i_d vs. $1/\{1+\exp[F/RT\,(E^0-E)]\}$ thus gives rise to a straight line. The slope of this line, $2.24\{(RT/Fv)^{1/2}\}.(2kC_A^0)^{1/2}$, provides immediate access to the value of k_{obs}. With Mn_{12}TH, $k_{obs} = 22.18\ s^{-1}$ was obtained from the slope at the very beginning of the catalytic process, and is independent of the scan rate [23] (see Figure S16 and Table T3). This value is about 630 times higher than the one calculated for Mn_{12}DH using the same method ($0.035\ s^{-1}$). This value is a remarkable result considering that the only difference between thb$^-$ and dhb$^-$ is that thb$^-$ has an additional OH group at its *para* position.

We then wished to understand the role of *para*OH in the high rate and low overpotential of the reaction. Recently, several plausible pathways for WO with transition-metal catalysts have been postulated.[24] Among these, the "water nucleophilic attack" pathway is one of the most common mechanisms proposed.[4,8,25] Accordingly, an initial Mn^{+3}-OH_2 $\rightarrow$ Mn^{+4}=O oxidation step should take place by a proton-coupled electron-transfer reaction, and this should further lead to oxygen production from water. Adopting this approach, and based on our electrochemical data, we propose the first two steps in this reaction catalyzed by Mn_{12}TH (Scheme 1). The CV of Mn_{12}TH (Figure 2 a, red line) shows an irreversible oxidation peak at 0.5 V, resulting from the oxidation of *para*OH [states (i) and (ii) in Scheme 1]. We believe that this oxidation is a key to the high reaction rate and low overpotential. It enables the formation of an ionic bond between $Mn1^{+3}$ and the carboxylate part of thb$^-$, and this ionic bond, which is anticipated to be stronger than the initial coordinate bond, should stabilize the formed $Mn1^{+4}$ ion in state (iii), thus facilitating the oxidation of $Mn1^{+3}$ to $Mn1^{+4}$ [state (ii) to state (iv) via state (iii) in Scheme 1]. A CV scan taken after 5 hours of CPE showed the two oxidation waves at 1 V and 1.67 V vs. NHE, but the oxidation wave at 0.5 V was missing (see Figure S17). This result supports the presence of state (ii) in solution, as the carbonyl group cannot be oxidized further. Current efforts in our group focus on isolating/synthesizing and characterizing some intermediates to support this proposed oxidation sequence and suggest a mechanism for the activity of Mn_{12}TH.

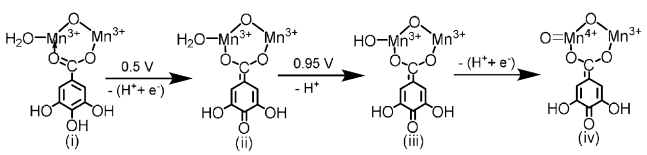

Scheme 1. Plausible initial oxidation sequence for WO by the Mn_{12}TH cluster in 0.1 M acetate buffer solution at pH 6. (i) One out of four identical units, within Mn_{12}TH, which is most likely responsible for catalysis, (ii) the oxidized form of (i) at 0.5 V vs. NHE, (iii), and (iv) the oxidized forms of (ii) at 0.95 V vs. NHE.

Notably, a CPE experiment done under the same conditions described above, but for 15 hours, revealed that oxygen evolution only occurs in the first 5 hours of the reaction (see Figure S18,19). Our continuous CV scan experiment and rinse tests of the electrode showed that no particles, typically decomposition products, are deposited on the electrode surface during the electrolysis. A CV scan, as well as UV/Vis, IR, and DLS measurements taken after 5 hours CPE of Mn_{12}TH showed that the waves, bands, and particle size are retained (see Figure S20,21). HRSEM and EDS analysis further support that there is no deposition of any particle or surface-bound material on the glassy carbon electrode surface. In contrast, a CV scan taken in acetate buffer solution at pH 4.9, which is the pH measured at the end of the 5 hour CPE experiment, was similar to the one taken in pH 6, showing all the redox waves, but the O_2 reduction wave at -0.5 V was missing (see Figure S22). In addition, the intensity of this CV was about three times lower than the intensity of the CV taken in pH 6. Adjusting the pH of the solution back to 6 did not restore its activity. According to these results, we can suggest that at pH < 5, some protonation event(s) takes place and lead to a permanent deactivation of the catalyst. Although 5 hours of catalytic activity is already a great achievement for such manganese-based clusters, which are typically active for only a few minutes,[26] we are currently investigating the source of our findings, aiming to develop efficient and longer-last electrocatalytic Mn-based clusters.

Disclosed here are the synthesis, characterization, and electrocatalytic WO activity of the highly water-soluble Mn_{12}TH cluster. This catalyst performs in 0.1 M acetate buffer at pH 6 with a TON of 13.2, high FE (93% in 5 hours), and an overpotential of only 74 mV, the lowest reported to date. We show that a slight change in the ligands bound to the Mn^{3+} ions results in a significant enhancement in the rate of the reaction and an increase in its FE. We suggest that the oxidation of the thb$^-$ ligand is playing a role in the catalytic activity by stabilizing the oxidation of Mn^{3+}, and might even assist in electron and proton shuttling within the WO process. This formidable effect of the ligands about the catalytic manganese center, which provide its second coordination sphere, on its catalytic activity is a conceptual advance in this field. We are currently investigating the mechanism of action of this catalyst to better understand this effect. We are also working towards improving the catalytic activity of this cluster, aiming to increase its duration of activity and TON, by

systematically modifying the ligand, and by developing new biomimetic metal clusters as efficient catalysts for water electrolysis and photolysis.

Acknowledgements

The authors thank Naama Gluz for fruitful discussions, Dr. Maria Koifman for the XRD measurements, and Dr. Rachel Edrei for the Elemental analysis and SEM measurements. This research was funded by the Solar Fuels Israel Center of Research Excellence (I-CORE) of the Israeli Science Foundation (ISF), grant number 2018762, and was supported by the Grand Technion Energy Program.

Conflict of interest

The authors declare no conflict of interest.

Keywords: electrochemistry · homogeneous catalysis · manganese · reaction mechanisms · water oxidation

How to cite: *Angew. Chem. Int. Ed.* **2019**, *58*, 2785 – 2790
Angew. Chem. **2019**, *131*, 2811 – 2816

[1] a) L. Chen, X. Dong, Y. Wang, Y. Xia, *Nat. Commun.* **2016**, *7*, 11741 – 11743; b) M. D. Kärkäs, O. Verho, E. V. Johnston, B. Åkermark, *Chem. Rev.* **2014**, *114*, 11863 – 12001; c) J. D. Blakemore, R. H. Crabtree, G. W. Brudvig, *Chem. Rev.* **2015**, *115*, 12974 – 13005; d) D. G. Nocera, *Acc. Chem. Res.* **2017**, *50*, 616 – 619.

[2] a) W. Lubitz, E. Reijerse, J. Messinger, *Energy Environ. Sci.* **2008**, *1*, 15 – 31; b) N. Cox, D. A. Pantazis, F. Neese, W. Lubitz, *Acc. Chem. Res.* **2013**, *46*, 1588 – 1596; c) S. Berardi, S. Drouet, L. Francas, C. Gimbert-Surinach, M. Guttentag, C. Richmond, T. Stoll, A. Llobet, *Chem. Soc. Rev.* **2014**, *43*, 7501 – 7519; d) B. M. Hunter, H. B. Gray, A. M. Muller, *Chem. Rev.* **2016**, *116*, 14120 – 14136.

[3] S. Liu, Y.-J. Lei, Z.-J. Xin, Y.-B. Lu, H.-Y. Wan, *J. Photochem. Photobiol. A* **2018**, *355*, 141 – 151.

[4] a) L. Duan, F. Bozoglian, S. Mandal, B. Stewart, T. Privalov, A. Llobet, L. Sun, *Nat. Chem.* **2012**, *4*, 418 – 423; b) J. J. Concepcion, M.-K. Tsai, J. T. Muckerman, T. J. Meyer, *J. Am. Chem. Soc.* **2010**, *132*, 1545 – 1557; c) V. Kunz, M. Schulze, D. Schmidt, F. Wurthner, *ACS Energy Lett.* **2017**, *2*, 288 – 293; d) D. W. Shaffer, Y. Xie, D. J. Szalda, J. J. Concepcion, *J. Am. Chem. Soc.* **2017**, *139*, 15347 – 15355.

[5] a) J. D. Blakemore, N. D. Schley, D. Balcells, J. F. Hull, G. W. Olack, C. D. Incarvito, O. Eisenstein, G. W. Brudvig, R. H. Crabtree, *J. Am. Chem. Soc.* **2010**, *132*, 16017 – 16029; b) C. Wang, J. L. Wang, W. Lin, *J. Am. Chem. Soc.* **2012**, *134*, 19895 – 19908.

[6] a) W. C. Ellis, N. D. McDaniel, S. Bernhard, T. J. Collins, *J. Am. Chem. Soc.* **2010**, *132*, 10990 – 10991; b) K. G. Kottrup, S. D'Agostini, P. H. Van Langevelde, M. A. Siegler, D. G. H. Hetterscheid, *ACS Catal.* **2018**, *8*, 1052 – 1061.

[7] a) D. J. Wasylenko, R. D. Palmer, E. Schott, C. P. Berlinguette, *Chem. Commun.* **2012**, *48*, 2107 – 2109; b) D. K. Dogutan, R. McGuire, D. G. Nocera, *J. Am. Chem. Soc.* **2011**, *133*, 9178 – 9180; c) J. B. Gerken, J. G. McAlpin, J. Y. C. Chen, M. L. Rigsby, W. H. Casey, R. D. Britt, S. S. Stahl, *J. Am. Chem. Soc.* **2011**, *133*, 14431 – 14442; d) M. W. Kanan, D. G. Nocera, *Science* **2008**, *321*, 1072 – 1075; e) H. Liu, M. Schilling, M. Yulikov, S. Luber, G. R. Patzke, *ACS Catal.* **2015**, *5*, 4994 – 4999; f) B. Zhang, F. Li, F. Yu, X. Wang, X. Zhou, X. Li, Y. Jiang, L. Sun, *ACS Catal.* **2014**, *4*, 804 – 809; g) J. Jiang, L. Huang, X. Liu, L. Ai, *ACS Appl. Mater. Interfaces* **2017**, *9*, 7193 – 7201.

[8] a) S. M. Barnett, K. I. Goldberg, J. M. Mayer, *Nat. Chem.* **2012**, *4*, 498 – 502; b) M. T. Zhang, Z. Chen, P. Kang, T. J. Meyer, *J. Am. Chem. Soc.* **2013**, *135*, 2048 – 2051; c) T. Ghosh, P. Ghosh, G. Maayan, *ACS Catal.* **2018**, *8*, 10631 – 10640; d) P. Garrido-Barros, I. Funes-Ardoiz, S. Drouet, J. Benet-Buchholz, F. Maseras, A. Llobet, *J. Am. Chem. Soc.* **2015**, *137*, 6758 – 6761; e) X. J. Su, M. Gao, L. Jiao, R. Z. Liao, P. E. M. Siegbahn, J. P. Cheng, M. T. Zhang, *Angew. Chem. Int. Ed.* **2015**, *54*, 4909 – 4914; *Angew. Chem.* **2015**, *127*, 4991 – 4996; f) K. J. Fisher, K. L. Materna, B. Q. Mercado, R. H. Crabtree, G. W. Brudvig, *ACS Catal.* **2017**, *7*, 3384 – 3387.

[9] a) R. E. Hansen, S. Das, *Energy Environ. Sci.* **2014**, *7*, 317 – 322; b) M. D. Kärkäs, B. Åkermark, *Dalton Trans.* **2016**, *45*, 14421 – 14461; c) E. A. Karlsson, B. L. Lee, T. Åkermark, E. V. Johnston, M. D. Kärkäs, J. Sun, Ö. Hansson, J. E. Bäckvall, B. Åkermark, *Angew. Chem. Int. Ed.* **2011**, *50*, 11715 – 11718; *Angew. Chem.* **2011**, *123*, 11919 – 11922; d) L. Ma, Q. Wang, W. L. Man, H. K. Kwong, C. C. Ko, T. C. Lau, *Angew. Chem. Int. Ed.* **2015**, *54*, 5246 – 5249; *Angew. Chem.* **2015**, *127*, 5335 – 5338; e) A. N. Radhakrishnan, P. P. Rao, K. S. M. Linsa, M. Deepa, P. Koshy, *Dalton Trans.* **2011**, *40*, 3839; f) R. Brimblecombe, G. F. Swiegers, G. C. Dismukes, L. Spiccia, *Angew. Chem. Int. Ed.* **2008**, *47*, 7335 – 7338; *Angew. Chem.* **2008**, *120*, 7445 – 7448; g) J. S. Bashkin, H.-R. Chang, W. E. Streib, J. C. Huffman, D. N. Hendrickson, G. Christou, *J. Am. Chem. Soc.* **1987**, *109*, 6502 – 6504; h) W. A. A. Arafa, M. D. Karkas, B.-L. Lee, T. Åkermark, R.-Z. Liao, H.-M. Berends, J. Messinger, P. E. M. Siegbahna, B. Åkermark, *Phys. Chem. Chem. Phys.* **2014**, *16*, 11950 – 11964; i) M. Yagi, K. Narita, *J. Am. Chem. Soc.* **2004**, *126*, 8084 – 8085; j) G. Berggren, A. Thapper, P. Huang, L. Eriksson, S. Styring, M. F. Anderlund, *Inorg. Chem.* **2011**, *50*, 3425 – 3430; k) Y. Yang, K. Mao, S. Gao, H. Huang, G. Xia, Z. Lin, P. Jiang, C. Wang, H. Wang, Q. Chen, *Adv. Mater.* **2018**, *30*, 1801732.

[10] a) Z. J. Liu, X. L. Wang, C. Qin, Z. M. Zhang, Y. G. Li, W. L. Chen, E. B. Wang, *Coord. Chem. Rev.* **2016**, *313*, 94 – 110; b) L. Sun, *Science* **2015**, *348*, 635 – 636.

[11] a) M. M. Najafpour, G. Renger, M. Hołyńska, A. N. Moghaddam, E. M. Aro, R. Carpentier, H. Nishihara, J. J. Eaton-Rye, J. R. Shen, S. I. Allakhverdiev, *Chem. Rev.* **2016**, *116*, 2886 – 2936; b) W. T. Lee, S. B. Muñoz, D. A. Dickie, J. M. Smith, *Angew. Chem. Int. Ed.* **2014**, *53*, 9856 – 9859; *Angew. Chem.* **2014**, *126*, 10014 – 10017; c) Y. Gao, R. H. Crabtree, G. W. Brudvig, *Inorg. Chem.* **2012**, *51*, 4043 – 4050; d) S. Kal, L. Ayensu-Mensah, P. H. Dinolfo, *Inorg. Chim. Acta* **2014**, *423*, 201 – 206.

[12] G. Maayan, N. Gluz, G. Christou, *Nat. Catal.* **2018**, *1*, 48 – 54.

[13] M. Soler, W. Wernsdorfer, Z. Sun, J. C. Huffman, D. N. Hendrickson, G. Christou, *Chem. Commun.* **2003**, 2672 – 2673.

[14] a) R. Sessoli, H.-L. Tsai, A. R. Schake, S. Wang, J. B. Vincent, K. Folting, D. Gatteschi, G. Christou, D. N. Hendrickson, *J. Am. Chem. Soc.* **1993**, *115*, 1804 – 1816; b) R. Bagai, G. Christou, *Chem. Soc. Rev.* **2009**, *38*, 1011 – 1026.

[15] a) H. A. Chu, H. Sackett, G. T. Babcock, *Biochemistry* **2000**, *39*, 14371 – 14376; b) H. A. Chu, W. Hillier, N. A. Law, G. T. Babcock, *Biochim. Biophys. Acta Bioenerg.* **2001**, *1503*, 69 – 82; c) N. Gluz, G. Maayan, *J. Coord. Chem.* **2018**, *71*, 1971 – 1984.

[16] S. Verma, A. Verma, A. K. Srivastava, A. Gupta, S. P. Singh, P. Singh, *Mater. Chem. Phys.* **2016**, *177*, 140 – 146.

[17] H. Schiller, H. Dau, *J. Photochem. Photobiol. B* **2000**, *55*, 138 – 144.

[18] a) L. P. Souza, F. Calegari, A. J. G. Zarbin, L. H. Marcolino-Júnior, M. F. Bergamini, *J. Agric. Food Chem.* **2011**, *59*, 7620 – 7625; b) J. H. Luo, B. L. Li, N. B. Li, H. Q. Luo, *Sens. Actuators B*

2013, *186*, 84 – 89; c) D. M. Stanković, M. Ognjanović, M. Fabian, L. Švorc, J. F. M. L. Mariano, B. Antić, *Anal. Biochem.* **2017**, *539*, 104 – 112; d) I. Ali, S. Omanovic, *Int. J. Electrochem. Sci.* **2013**, *8*, 4283 – 4304.

[19] a) H. Lund, O. Hammerich, *Organic Electrochemistry*, 4th ed., Dekker, New York, **2001**; b) C. W. Lange, C. G. Pierpont, *Inorg. Chim. Acta* **1997**, *263*, 219 – 224; c) C. G. Pierpont, R. M. Buchanan, *Coord. Chem. Rev.* **1981**, *38*, 45 – 87.

[20] N. Kaeffer, A. Morozan, J. Fize, E. Martinez, L. Guetaz, V. Artero, *ACS Catal.* **2016**, *6*, 3727 – 3737.

[21] a) E. S. Rountree, B. D. McCarthy, T. T. Eisenhart, J. L. Dempsey, *Inorg. Chem.* **2014**, *53*, 9983 – 10002; b) C. Costentin, S. Drouet, M. Robert, J. M. Saveant, *J. Am. Chem. Soc.* **2012**, *134*, 11235 – 11242.

[22] J. M. Savéant, *Elements of Molecular and Biomolecular Electrochemistry: An Electrochemical Approach to Electron Transfer Chemistry*, Wiley, New York, **2000**.

[23] a) C. Costentin, G. Passard, J.-M. Savéant, *J. Am. Chem. Soc.* **2015**, *137*, 5461 – 5467; b) A. J. Bard, L. R. Faulkner, *Electrochemical Methods: Fundamentals and Applications*, 2nd ed., Wiley, New York, **2000**.

[24] a) H. Dau, C. Limberg, T. Reier, M. Risch, S. Roggan, P. Strasser, *ChemCatChem* **2010**, *2*, 724 – 761; b) X. Sala, S. Maji, R. Bofill, J. García-Anton, L. Escriche, A. Llobet, *Acc. Chem. Res.* **2014**, *47*, 504 – 516; c) T. J. Meyer, M. V. Sheridan, B. D. Sherman, *Chem. Soc. Rev.* **2017**, *46*, 6148 – 6169.

[25] a) T. F. Hughes, R. A. Friesner, *J. Phys. Chem. B* **2011**, *115*, 9280 – 9289; b) S. Khan, K. R. Yang, M. Z. Ertem, V. S. Batista, G. W. Brudvig, *ACS Catal.* **2015**, *5*, 7104 – 7113; c) B. Rudshteyn, K. J. Fisher, H. M. C. Lant, K. R. Yang, B. Q. Mercado, G. W. Brudvig, R. H. Crabtree, V. S. Batista, *ACS Catal.* **2018**, *8*, 7952 – 7960.

[26] Y. Yan, J. S. Lee, D. A. Ruddy, *Inorg. Chem.* **2015**, *54*, 4550 – 4555.

Manuscript received: December 6, 2018
Revised manuscript received: January 3, 2019
Version of record online: January 29, 2019

Electrochemistry

International Edition: DOI: 10.1002/anie.201813895
German Edition: DOI: 10.1002/ange.201813895

Efficient Homogeneous Electrocatalytic Water Oxidation by a Manganese Cluster with an Overpotential of Only 74 mV

*Totan Ghosh and Galia Maayan**

Abstract: *Water electrolysis is among the simplest method for generating hydrogen as an alternative renewable fuel. A major challenge associated with this process is the development of cheap, simple, and environmentally benign catalysts that lead to a minimum overpotential for water oxidation. Inspired by the Mn_4CaO_x cluster that catalyzes water oxidation in photosystem II, described here is the synthesis and characterization of the manganese cluster $[Mn_{12}O_{12}(O_2CC_6H_2(OH)_3)_{16}(H_2O)_4]$ ($Mn_{12}TH$) along with its electrocatalytic activity at pH 6. Electrochemical, spectroscopic, and electron microscopy studies show that $Mn_{12}TH$ is a homogeneous electrocatalyst for water oxidation and enables oxygen evolution with a reaction rate of 22 s^{-1}, high Faradic efficiency (93 %), and an overpotential of only 74 mV, the lowest reported to date. Based on the electrochemical data, the organic ligands, which can be described as the second coordination sphere of the catalytic manganese core, play a key role in facilitating the oxidation process and accelerating the reaction.*

One of the promising approaches for clean fuel generation is water splitting to produce molecular oxygen and hydrogen, the latter being a renewable energy source.[1] The production of molecular hydrogen from water involves two half reactions: 1) water oxidation: $2H_2O = O_2 + 4H^+ + 4e^-$ and 2) proton reduction: $2H^+ + 2e^- = H_2$. From these two, water oxidation (WO) is the bottleneck of the whole water splitting process because of the transfer of multiple protons and electrons and the very high thermodynamic potential required for this reaction [$E^0 = 1.23$ V vs. normal hydrogen electrode (NHE), $E_{pH\,6} = 0.876$ V vs. NHE].[2] Over the years, many heterogeneous WO catalysts have been developed.[3] Compared to heterogeneous catalysts, homogeneous systems enable rational design of molecular catalysts, facilitate understanding of reaction mechanism, and can be systematically tuned and optimized. Given these advantages, several transition-metal complexes have been developed as homogeneous catalysts for WO and are based on the metal ions Ru,[4] Ir,[5] Fe,[6] Co,[7] Cu,[8] and Mn.[9] Further advances require the development of catalysts that are not only based on earth-abundant metals, but are also stable, fast and, most importantly, can perform with as low overpotential as possible to meet practical applications. One approach to address these goals is to mimic the structure and function of the oxygen-evolving complex (OEC) in photosystem II (PSII), which is a manganese-oxo cluster. Although various structural mimics of the OEC are reported,[10] manganese-based homogeneous water oxidation electrocatalysts are very scant.[11] Recently, our group reported the water-soluble manganese-based electrocatalyst $[Mn_{12}O_{12}(O_2CC_6H_3(OH)_2)_{16}(H_2O)_4]$ ($Mn_{12}DH$),[12] which structurally mimics the OEC and operates at pH 6 with a low overpotential of only 334 mV, average k_{obs} of 0.035 s^{-1} (based on Foot-of-the-wave analysis, FOWA), and Faradic efficiency (FE) of 80 % (see Table T1 in the Supporting Information). We suggested that the hydroxy groups on the organic ligands, which can be described as the second coordination sphere of the manganese catalyst, may contribute to the catalysis by either proton transfer or shuttling and/or by facilitating the formation of high-valence species required for water oxidation. To probe the role of the hydroxy substituent in the electrocatalytic activity, aiming to increase the rate and efficiency of the reaction and to lower its overpotential even further, we are currently developing similar manganese clusters from different organic ligands.

Herein we describe the successful synthesis of a new cluster, $[Mn_{12}O_{12}(O_2CC_6H_2(OH)_3)_{16}(H_2O)_4]$ ($Mn_{12}TH$, Figure 1 a), which is based on the ligand 3,4,5-trihydroxy benzoic acid (thbH), and its electrocatalytic WO activity. We have discovered that this small change in the second coordination sphere about the metal center leads to almost three orders of magnitude faster ($k_{obs} = 22$ s^{-1}) and highly efficient (93 % FE) catalytic water oxidation activity at pH 6 with an overpotential of only 74 mV. This value is the lowest overpotential reported for homogeneous a WO electrocatalyst by any first-row transition-metal complex to date (see Table T2). Based

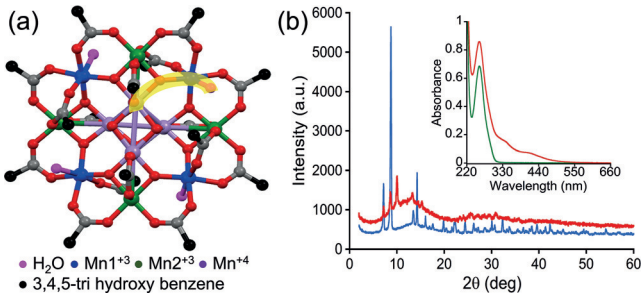

Figure 1. a) Suggested structure of $[Mn_{12}O_{12}(O_2CC_6H_2(OH)_3)_{16}(H_2O)_4]$ ($Mn_{12}TH$) viewed along the molecular *x* axis. The Mn^{4+}-*O*-$Mn1^{3+}$-H_2O motif is highlighted in yellow. Hydrogen atoms are omitted for clarity. The structure was adapted from Ref. [13]. b) Powder XRD pattern of the cluster $Mn_{12}TH$ (red line) and $Mn_{12}Ac$ (blue line). Inset: UV/Vis spectrum of the complex $Mn_{12}TH$ (red line) and thbH ligand (green line).

[*] Dr. T. Ghosh, Prof. G. Maayan
Schulich Faculty of Chemistry, Technion-Israel Institute of Technology
Technion City, Haifa 3200008 (Israel)
E-mail: gm92@technion.ac.il
Supporting information and the ORCID identification number(s) for the author(s) of this article can be found under: https://doi.org/10.1002/anie.201813895.

on the pH-dependent redox properties of thbH and $Mn_{12}TH$, and on our electrochemical data, we propose the first two steps of the reaction with $Mn_{12}TH$ and suggest that the oxidation of the additional OH group by the applied potential assists in stabilizing the higher oxidation state of the catalytic manganese ion, thus enhancing the reaction rate and lowering the overpotential.

The highly water-soluble $Mn_{12}TH$ cluster was prepared in aqueous medium by adopting, with some modifications, the synthetic procedure used for the synthesis of $[Mn_{12}O_{12}(O_2CCH_3)_{16}(H_2O)_4]$ ($Mn_{12}Ac$)[14]. The full synthesis is described in the Supporting Information. $Mn_{12}TH$ was characterized by a collection of different analytical methods. The IR spectrum showed some distinct peaks in the range of $\upsilon = 610$–$720\ cm^{-1}$ corresponding to the various Mn–O stretching modes and at $\upsilon = 1023$, $1041\ cm^{-1}$ for the Ar-O-H stretching frequencies.[15] This spectrum was further compared to the IR spectrum of $[Mn_{12}O_{12}(O_2CC_6H_5)_{16}(H_2O)_4]$ ($Mn_{12}Bz$), which we synthesized according to a literature method.[14] The high similarity between the two spectra, specifically in the region of the carboxylate bands ($\upsilon = 2000$–$1000\ cm^{-1}$), suggests that $Mn_{12}TH$ retains the $[Mn_{12}O_{12}(O_2CR)_{16}(H_2O)_4]$ structure (see Figure S2). This structure was further supported by powder XRD analysis showing diffraction peaks at 2θ values of 7.17, 8.96, 10.06, and 13.66, consistent with the reported powder XRD pattern of Mn_{12} stearate[16] and of pure crystals of $Mn_{12}Ac$ synthesized in our lab (Figure 1b). Additionally, the ESI-MS analysis of $Mn_{12}TH$ in water showed a peak at 3627.1 (cal. Mw = 3627.46) corresponding to the full mass of the cluster (see Figure S3). Furthermore, the UV/Vis spectrum of $Mn_{12}TH$ showed an absorption band near $\lambda_{max} = 260$ nm corresponding to the π–π* transition of thbH and two broad bands near $\lambda = 335$ nm and 420 nm, which arise from the ligand-to-metal charge-transfer transition and metal d–d transition, respectively (Figure 1b, inset). Experimental data from a C, H, N analysis indicated the presence of 20 water molecules outside the cluster moiety. Thermogravimetric analysis supported these results, showing that 9.6% weight loss is taking place in the temperature range between 90 °C and 150 °C (see Figure S4), and is in agreement with the calculated weight loss (9.03%) for 20 water molecules. Collectively, the experimental analysis provides strong evidence for the formation of the $Mn_{12}TH$ structure as shown in Figure 1a.

Cyclic voltamograms (CVs) of thbH and $Mn_{12}TH$ were performed in aqueous acetate buffer at pH 6.0, the pH at which the OEC within PSII shows optimal catalytic performance,[17] and at which $Mn_{12}TH$ was found to be stable for a long time. The CV of thbH shows two oxidation waves at 0.7 V and 0.95 V vs. NHE (Figure 2a, black line). These waves are attributed to the oxidation of the *para* OH group (*para*OH) to form a semiquinone radical, followed by the oxidation of a *meta* OH group to form a quinone, respectively (see Scheme S1).[18] Both processes involve one proton and one electron oxidation each, with no peaks on the reverse scan, indicating that this process is irreversible, as previously demonstrated.[18,19] We note here, that the pH-dependence study of thbH is also well described in the literature, showing that the peak potential shifts to a lower potential region as the

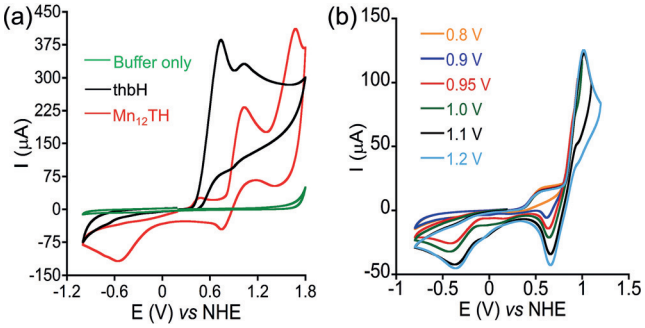

Figure 2. a) CV scans of a 0.1 M acetate buffer at pH 6 (green line), with 0.5 mM thbH (black line) and with 0.5 mM $Mn_{12}TH$ (red line) using a glassy carbon electrode ($S = 0.07\ cm^2$). b) CV scans of $Mn_{12}TH$ in 0.1 M acetate buffer pH 6 taken at different potential ranges.

pH is increased from 2 to 7, indicating that the electrode process is influenced by the protonation reactions.[18] The CV of $Mn_{12}TH$ at pH 6, scanning in the anodic direction, shows three oxidation waves at $E_p = 0.5$, 1.0, and 1.67 V vs. NHE and two reduction peaks at $E_p = 0.75$ and −0.5 V vs. NHE (Figure 2a, red line). The first oxidation wave is assigned to the oxidation of the *para*OH, the second and third waves at 1.0 V and 1.67 V, respectively, can be each assigned to the oxidation of one Mn^{+3} to Mn^{+4}.[14b] As the carboxylate group of thb^- is bonded to the manganese ion(s), the oxidation of the *para*OH is further facilitated and hence takes place at lower potential compared to the same oxidation within thbH (0.5 vs. 0.7 V). The absence of a corresponding reduction peak suggests that the oxidation of *para*OH within $Mn_{12}TH$ is also irreversible. The pH-dependent reduction peak at 0.75 V could be assigned to the reduction of Mn^{+4}=O to Mn^{+3}-OH. The new reduction peak at −0.5 V could be assigned to the reduction of produced O_2 to O_2^-,[12] suggesting that the oxidation of $Mn_{12}TH$ triggers electrocatalytic WO to O_2. To verify that the reduction peak at −0.5 V corresponds to the O_2/O_2^- reduction, we reversed the CV scan direction after purging the solution with argon gas and scanned first in the cathodic direction from 0 to −1.0 V and then continued to the anodic direction until 1.7 V vs. Ag/AgCl. This CV experiment showed that the −0.5 V feature was absent in the first cycle but appeared again in the following cycle, indicating that it arises from the high-potential oxidation process, in which oxygen is being produced (see Figure S5).[8a,12]

The pH-dependent CV study performed with $Mn_{12}TH$ at pH 4–7 showed that the intensity and oxidation potential of the wave at 1.0 V at pH 6 and 7 are very similar. When decreasing the pH to 5 and then to 4, this oxidation wave shifts towards higher potential and its intensity decreases significantly at pH 4 (see Figure S6a). The slope of $129\ mV\ pH^{-1}$ obtained from plotting the E (V) against the pH suggests that the oxidation at 0.95 V takes place by a loss of two protons (see Figure S6b).[18,19]

To find out the minimum potential at which evolution of oxygen occurs, we performed CV experiments with $Mn_{12}TH$, scanning at $100\ mV\ s^{-1}$ from 0 to 0.8 (which is the onset potential for the oxidation of the first Mn^{3+} to Mn^{4+}), 0.9, 0.95, 1, 1.1 and 1.2 V vs. NHE (Figure 2b). The CV data showed that oxygen evolution takes place already at a potential as low

as 0.95 V vs. NHE, by the appearance of the wave at −0.45 V vs. NHE, which corresponds to the O_2/O_2^- couple.[12] The shift in reduction potential from −0.5 to −0.45 V suggests that the oxidation process is diffusion controlled.

Controlled potential electrolysis (CPE) was therefore performed at 0.75 V vs. Ag/AgCl (0.95 V vs. NHE) to quantify the total evolved oxygen. Evolution of molecular oxygen was investigated by a 5 hour CPE experiment with a porous glassy carbon working electrode in 0.1 M acetate buffer solution, at pH 6, containing 5 mL of 0.5 mM Mn_{12}TH. This electrolysis experiment afforded a total of 157 μM of oxygen, which is 32.5 μmole in 5 hours of electrolysis in 0.1 M acetate buffer at pH 6 (Figure 3a). The total accumulated

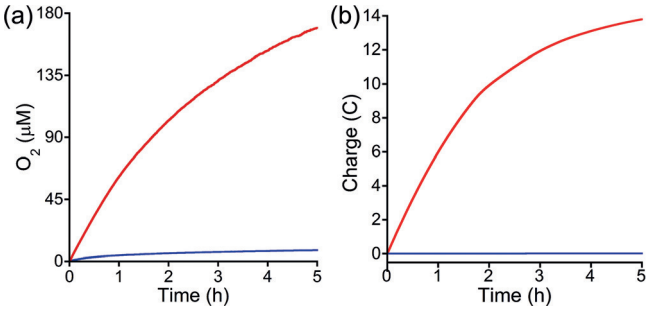

Figure 3. a) Evolution of O_2 measured with a fluorescence probe and b) Total accumulated charge during CPE, both from a solution containing 0.5 mM Mn_{12}TH (red lines), and the buffer only (blue lines), using a porous carbon working electrode at 0.95 V vs. NHE. All solutions contained 0.1 M acetate buffer at pH 6.

charge during this process was 13.8 C (Figure 3b). Based on a 4 e^- process and initial amount of catalyst in solution, the FE and the catalytic TON were calculated to be 93% and 13.2 in 5 hours, respectively (see details in the Supporting Information). The pH of the solution measured at the end of the reaction was 4.9, consistent with the production of protons during electrocatalytic WO.[8b,c] The overpotential for this catalytic process was only 74 mV, the lowest in homogeneous electrocatalytic WO reactions reported to date (see Table T2).

To investigate whether the catalytic process is truly homogeneous, we performed a CV scan in acetate buffer at pH 6 in the absence of Mn_{12}TH, added the cluster, and performed 25 continuous CV scans, and then took out the electrode and rinsed it with water without polishing it. This electrode was then placed in an acetate buffer solution at pH 6 that did not contain Mn_{12}TH, and another CV scan was performed (see Figure S8,S9). This scan was almost identical to the first one taken in the absence of the cluster, suggesting no deposition of the catalyst on the electrode surface. Moreover, the CV scan of the first cycle is also almost identical to that of the 25th cycle, with the only difference being the wave at 0.5 V, which is missing in the 25th cycle because of the irreversible oxidation of thb^-. Additionally, we performed another rinse test, according to Artero et al.,[20] in which we took out the glassy carbon electrode after 25 continuous CV scans, dried it in air without rinsing or polishing its surface, dipped it in 0.1 M acetate buffer solution at pH 6, and ran another CV scan. The obtained voltamogram (blue line, Figure 4a) was also almost identical to this of the blank buffer solution (green line, Figure 4a). Overall, these CV measurements suggest that there is no deposition of any

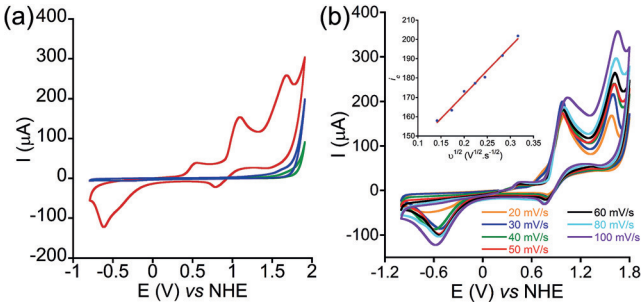

Figure 4. a) CVs of 0.1 M acetate buffer solution at pH 6 in the absence of Mn_{12}TH (green), in the presence of Mn_{12}TH (red), and in the absence of Mn_{12}TH but with the electrode used for 25 scans in the presence of Mn_{12}TH, which was neither rinsed nor polished (blue). b) CVs of a 0.5 mM Mn_{12}TH in different scan rates using a glassy carbon electrode ($S = 0.07$ cm^2, pH 6, 0.1 M acetate buffer). Inset: a plot of the catalytic peak current (i_c) vs. the square root of the scan rate ($R = 0.99$).

particle on the working electrode surface and that Mn_{12}TH is a stable catalyst in solution. To support this conclusion, SEM analysis of the working glassy carbon electrode, before and after the 25 scans, was performed and further confirmed that no particles were adsorbed on the electrode surface (see Figure S10). HRSEM analysis of the glassy carbon electrode before (see Figure S11) and after 5 h of a control potential electrolysis (see Figure S12) also showed that there is no deposition of any particle on the electrode surface. In addition, DLS analyses of the Mn_{12}TH cluster before and after 5 hours of electrolysis in 0.1 M acetate buffer solution (see Figure S13) showed that the particle distribution is in the range of 0.9–1.5 nm, which is the molecular hydrodynamic diameter of the cluster only, indicating that there is no formation of new particles taking place during electrolysis. Collectively, these experiments strongly suggest that Mn_{12}TH is a truly homogeneous WO electrocatalyst.

Additionally, CVs were recorded at different scan rates (Figure 4b) to verify that the catalytic process is diffusion controlled (thus homogeneous). We examined the scan rate dependence oxidation currents at −0.5 V, 1.0 V, and 1.67 V vs. NHE respectively in 0.1 M acetate buffers at pH 6 and obtained a linear fit when the intensity at the peak of each oxidation event was plotted against the square root of the scan rate (Figure 4b, see Figures S14 and S15). These results indicate that the oxidation currents are diffusion controlled and the catalytic process is truly homogeneous.

To find out the k_{obs} value of this catalytic reaction we followed a methodology that was developed by Saveant et al. for electrocatalytic processes, known as foot-of-the-wave analysis (FOWA).[21] Considering no side-phenomenon perturbs the catalytic reaction (at the very beginning of it), the reaction is fast as compared to Fv/RT, in which v is the scan rate, thus it is independent of scan rate and can be described by the following equation:

$$\frac{i}{FS} = \frac{Cp^0\sqrt{Dp2kC_A^0}}{1+\exp\left[\frac{F}{RT}(E-E^0)\right]} \quad (1)$$

The peak current of the catalyst in the absence of substrate[22] may serve to calibrate the catalytic response in terms of electrode surface area, S, catalyst concentration, C_p^0, diffusion coefficient, D_p, and scan rate, ν.

$$\frac{i_p^0}{FS} = 0.446Cp^0\sqrt{Dp.}\sqrt{\frac{Fv}{RT}} \quad (2)$$

It is thus convenient to observe the variation of i/i_p^0 as:

$$\frac{i}{i_p^0} = \frac{2.24\sqrt{\frac{RT}{Fv}2kC_A^0}}{1+\exp\left[\frac{F}{RT}(E-E^0)\right]} \quad (3)$$

Here i_c, catalytic peak current at 0.95 V; i_d, non- catalytic peak current at 0.75 V; $E^0 = 0.95$ V, k = catalytic rate constant = $k_{obs.}$

Plotting i_c/i_d vs. $1/\{1+\exp[F/RT\,(E^0-E)]\}$ thus gives rise to a straight line. The slope of this line, $2.24\{(RT/Fv)^{1/2}\}\cdot(2kC_A^0)^{1/2}$, provides immediate access to the value of k_{obs}. With Mn_{12}TH, $k_{obs} = 22.18\ s^{-1}$ was obtained from the slope at the very beginning of the catalytic process, and is independent of the scan rate [23] (see Figure S16 and Table T3). This value is about 630 times higher than the one calculated for Mn_{12}DH using the same method ($0.035\ s^{-1}$). This value is a remarkable result considering that the only difference between thb$^-$ and dhb$^-$ is that thb$^-$ has an additional OH group at its *para* position.

We then wished to understand the role of *para*OH in the high rate and low overpotential of the reaction. Recently, several plausible pathways for WO with transition-metal catalysts have been postulated.[24] Among these, the "water nucleophilic attack" pathway is one of the most common mechanisms proposed.[4,8,25] Accordingly, an initial Mn^{+3}-OH_2 → Mn^{+4}=O oxidation step should take place by a proton-coupled electron-transfer reaction, and this should further lead to oxygen production from water. Adopting this approach, and based on our electrochemical data, we propose the first two steps in this reaction catalyzed by Mn_{12}TH (Scheme 1). The CV of Mn_{12}TH (Figure 2 a, red line) shows an irreversible oxidation peak at 0.5 V, resulting from the oxidation of *para*OH [states (i) and (ii) in Scheme 1]. We believe that this oxidation is a key to the high reaction rate and low overpotential. It enables the formation of an ionic bond between $Mn1^{+3}$ and the carboxylate part of thb$^-$, and this ionic bond, which is anticipated to be stronger than the initial coordinate bond, should stabilize the formed $Mn1^{+4}$ ion in state (iii), thus facilitating the oxidation of $Mn1^{+3}$ to $Mn1^{+4}$ [state (ii) to state (iv) via state (iii) in Scheme 1]. A CV scan taken after 5 hours of CPE showed the two oxidation waves at 1 V and 1.67 V vs. NHE, but the oxidation wave at 0.5 V was missing (see Figure S17). This result supports the presence of state (ii) in solution, as the carbonyl group cannot be oxidized further. Current efforts in our group focus on isolating/synthesizing and characterizing some intermediates to support this proposed oxidation sequence and suggest a mechanism for the activity of Mn_{12}TH.

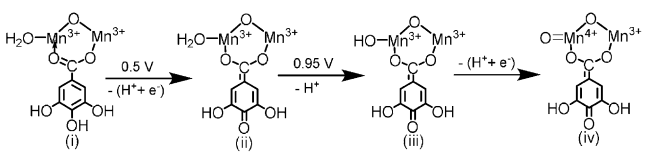

Scheme 1. Plausible initial oxidation sequence for WO by the Mn_{12}TH cluster in 0.1 M acetate buffer solution at pH 6. (i) One out of four identical units, within Mn_{12}TH, which is most likely responsible for catalysis, (ii) the oxidized form of (i) at 0.5 V vs. NHE, (iii), and (iv) the oxidized forms of (ii) at 0.95 V vs. NHE.

Notably, a CPE experiment done under the same conditions described above, but for 15 hours, revealed that oxygen evolution only occurs in the first 5 hours of the reaction (see Figure S18,19). Our continuous CV scan experiment and rinse tests of the electrode showed that no particles, typically decomposition products, are deposited on the electrode surface during the electrolysis. A CV scan, as well as UV/Vis, IR, and DLS measurements taken after 5 hours CPE of Mn_{12}TH showed that the waves, bands, and particle size are retained (see Figure S20,21). HRSEM and EDS analysis further support that there is no deposition of any particle or surface-bound material on the glassy carbon electrode surface. In contrast, a CV scan taken in acetate buffer solution at pH 4.9, which is the pH measured at the end of the 5 hour CPE experiment, was similar to the one taken in pH 6, showing all the redox waves, but the O_2 reduction wave at −0.5 V was missing (see Figure S22). In addition, the intensity of this CV was about three times lower than the intensity of the CV taken in pH 6. Adjusting the pH of the solution back to 6 did not restore its activity. According to these results, we can suggest that at pH < 5, some protonation event(s) takes place and lead to a permanent deactivation of the catalyst. Although 5 hours of catalytic activity is already a great achievement for such manganese-based clusters, which are typically active for only a few minutes,[26] we are currently investigating the source of our findings, aiming to develop efficient and longer-last electrocatalytic Mn-based clusters.

Disclosed here are the synthesis, characterization, and electrocatalytic WO activity of the highly water-soluble Mn_{12}TH cluster. This catalyst performs in 0.1 M acetate buffer at pH 6 with a TON of 13.2, high FE (93% in 5 hours), and an overpotential of only 74 mV, the lowest reported to date. We show that a slight change in the ligands bound to the Mn^{3+} ions results in a significant enhancement in the rate of the reaction and an increase in its FE. We suggest that the oxidation of the thb$^-$ ligand is playing a role in the catalytic activity by stabilizing the oxidation of Mn^{3+}, and might even assist in electron and proton shuttling within the WO process. This formidable effect of the ligands about the catalytic manganese center, which provide its second coordination sphere, on its catalytic activity is a conceptual advance in this field. We are currently investigating the mechanism of action of this catalyst to better understand this effect. We are also working towards improving the catalytic activity of this cluster, aiming to increase its duration of activity and TON, by

systematically modifying the ligand, and by developing new biomimetic metal clusters as efficient catalysts for water electrolysis and photolysis.

Acknowledgements

The authors thank Naama Gluz for fruitful discussions, Dr. Maria Koifman for the XRD measurements, and Dr. Rachel Edrei for the Elemental analysis and SEM measurements. This research was funded by the Solar Fuels Israel Center of Research Excellence (I-CORE) of the Israeli Science Foundation (ISF), grant number 2018762, and was supported by the Grand Technion Energy Program.

Conflict of interest

The authors declare no conflict of interest.

Keywords: electrochemistry · homogeneous catalysis · manganese · reaction mechanisms · water oxidation

How to cite: *Angew. Chem. Int. Ed.* **2019**, *58*, 2785 – 2790
Angew. Chem. **2019**, *131*, 2811 – 2816

[1] a) L. Chen, X. Dong, Y. Wang, Y. Xia, *Nat. Commun.* **2016**, *7*, 11741 – 11743; b) M. D. Kärkäs, O. Verho, E. V. Johnston, B. Åkermark, *Chem. Rev.* **2014**, *114*, 11863 – 12001; c) J. D. Blakemore, R. H. Crabtree, G. W. Brudvig, *Chem. Rev.* **2015**, *115*, 12974 – 13005; d) D. G. Nocera, *Acc. Chem. Res.* **2017**, *50*, 616 – 619.

[2] a) W. Lubitz, E. Reijerse, J. Messinger, *Energy Environ. Sci.* **2008**, *1*, 15 – 31; b) N. Cox, D. A. Pantazis, F. Neese, W. Lubitz, *Acc. Chem. Res.* **2013**, *46*, 1588 – 1596; c) S. Berardi, S. Drouet, L. Francas, C. Gimbert-Surinach, M. Guttentag, C. Richmond, T. Stoll, A. Llobet, *Chem. Soc. Rev.* **2014**, *43*, 7501 – 7519; d) B. M. Hunter, H. B. Gray, A. M. Muller, *Chem. Rev.* **2016**, *116*, 14120 – 14136.

[3] S. Liu, Y.-J. Lei, Z.-J. Xin, Y.-B. Lu, H.-Y. Wan, *J. Photochem. Photobiol. A* **2018**, *355*, 141 – 151.

[4] a) L. Duan, F. Bozoglian, S. Mandal, B. Stewart, T. Privalov, A. Llobet, L. Sun, *Nat. Chem.* **2012**, *4*, 418 – 423; b) J. J. Concepcion, M.-K. Tsai, J. T. Muckerman, T. J. Meyer, *J. Am. Chem. Soc.* **2010**, *132*, 1545 – 1557; c) V. Kunz, M. Schulze, D. Schmidt, F. Wurthner, *ACS Energy Lett.* **2017**, *2*, 288 – 293; d) D. W. Shaffer, Y. Xie, D. J. Szalda, J. J. Concepcion, *J. Am. Chem. Soc.* **2017**, *139*, 15347 – 15355.

[5] a) J. D. Blakemore, N. D. Schley, D. Balcells, J. F. Hull, G. W. Olack, C. D. Incarvito, O. Eisenstein, G. W. Brudvig, R. H. Crabtree, *J. Am. Chem. Soc.* **2010**, *132*, 16017 – 16029; b) C. Wang, J. L. Wang, W. Lin, *J. Am. Chem. Soc.* **2012**, *134*, 19895 – 19908.

[6] a) W. C. Ellis, N. D. McDaniel, S. Bernhard, T. J. Collins, *J. Am. Chem. Soc.* **2010**, *132*, 10990 – 10991; b) K. G. Kottrup, S. D'Agostini, P. H. Van Langevelde, M. A. Siegler, D. G. H. Hetterscheid, *ACS Catal.* **2018**, *8*, 1052 – 1061.

[7] a) D. J. Wasylenko, R. D. Palmer, E. Schott, C. P. Berlinguette, *Chem. Commun.* **2012**, *48*, 2107 – 2109; b) D. K. Dogutan, R. McGuire, D. G. Nocera, *J. Am. Chem. Soc.* **2011**, *133*, 9178 – 9180; c) J. B. Gerken, J. G. McAlpin, J. Y. C. Chen, M. L. Rigsby, W. H. Casey, R. D. Britt, S. S. Stahl, *J. Am. Chem. Soc.* **2011**, *133*, 14431 – 14442; d) M. W. Kanan, D. G. Nocera, *Science* **2008**, *321*, 1072 – 1075; e) H. Liu, M. Schilling, M. Yulikov, S. Luber, G. R. Patzke, *ACS Catal.* **2015**, *5*, 4994 – 4999; f) B. Zhang, F. Li, F. Yu, X. Wang, X. Zhou, X. Li, Y. Jiang, L. Sun, *ACS Catal.* **2014**, *4*, 804 – 809; g) J. Jiang, L. Huang, X. Liu, L. Ai, *ACS Appl. Mater. Interfaces* **2017**, *9*, 7193 – 7201.

[8] a) S. M. Barnett, K. I. Goldberg, J. M. Mayer, *Nat. Chem.* **2012**, *4*, 498 – 502; b) M. T. Zhang, Z. Chen, P. Kang, T. J. Meyer, *J. Am. Chem. Soc.* **2013**, *135*, 2048 – 2051; c) T. Ghosh, P. Ghosh, G. Maayan, *ACS Catal.* **2018**, *8*, 10631 – 10640; d) P. Garrido-Barros, I. Funes-Ardoiz, S. Drouet, J. Benet-Buchholz, F. Maseras, A. Llobet, *J. Am. Chem. Soc.* **2015**, *137*, 6758 – 6761; e) X. J. Su, M. Gao, L. Jiao, R. Z. Liao, P. E. M. Siegbahn, J. P. Cheng, M. T. Zhang, *Angew. Chem. Int. Ed.* **2015**, *54*, 4909 – 4914; *Angew. Chem.* **2015**, *127*, 4991 – 4996; f) K. J. Fisher, K. L. Materna, B. Q. Mercado, R. H. Crabtree, G. W. Brudvig, *ACS Catal.* **2017**, *7*, 3384 – 3387.

[9] a) R. E. Hansen, S. Das, *Energy Environ. Sci.* **2014**, *7*, 317 – 322; b) M. D. Kärkäs, B. Åkermark, *Dalton Trans.* **2016**, *45*, 14421 – 14461; c) E. A. Karlsson, B. L. Lee, T. Åkermark, E. V. Johnston, M. D. Kärkäs, J. Sun, Ö. Hansson, J. E. Bäckvall, B. Åkermark, *Angew. Chem. Int. Ed.* **2011**, *50*, 11715 – 11718; *Angew. Chem.* **2011**, *123*, 11919 – 11922; d) L. Ma, Q. Wang, W. L. Man, H. K. Kwong, C. C. Ko, T. C. Lau, *Angew. Chem. Int. Ed.* **2015**, *54*, 5246 – 5249; *Angew. Chem.* **2015**, *127*, 5335 – 5338; e) A. N. Radhakrishnan, P. P. Rao, K. S. M. Linsa, M. Deepa, P. Koshy, *Dalton Trans.* **2011**, *40*, 3839; f) R. Brimblecombe, G. F. Swiegers, G. C. Dismukes, L. Spiccia, *Angew. Chem. Int. Ed.* **2008**, *47*, 7335 – 7338; *Angew. Chem.* **2008**, *120*, 7445 – 7448; g) J. S. Bashkin, H.-R. Chang, W. E. Streib, J. C. Huffman, D. N. Hendrickson, G. Christou, *J. Am. Chem. Soc.* **1987**, *109*, 6502 – 6504; h) W. A. A. Arafa, M. D. Karkas, B.-L. Lee, T. Åkermark, R.-Z. Liao, H.-M. Berends, J. Messinger, P. E. M. Siegbahna, B. Åkermark, *Phys. Chem. Chem. Phys.* **2014**, *16*, 11950 – 11964; i) M. Yagi, K. Narita, *J. Am. Chem. Soc.* **2004**, *126*, 8084 – 8085; j) G. Berggren, A. Thapper, P. Huang, L. Eriksson, S. Styring, M. F. Anderlund, *Inorg. Chem.* **2011**, *50*, 3425 – 3430; k) Y. Yang, K. Mao, S. Gao, H. Huang, G. Xia, Z. Lin, P. Jiang, C. Wang, H. Wang, Q. Chen, *Adv. Mater.* **2018**, *30*, 1801732.

[10] a) Z. J. Liu, X. L. Wang, C. Qin, Z. M. Zhang, Y. G. Li, W. L. Chen, E. B. Wang, *Coord. Chem. Rev.* **2016**, *313*, 94 – 110; b) L. Sun, *Science* **2015**, *348*, 635 – 636.

[11] a) M. M. Najafpour, G. Renger, M. Hołyńska, A. N. Moghaddam, E. M. Aro, R. Carpentier, H. Nishihara, J. J. Eaton-Rye, J. R. Shen, S. I. Allakhverdiev, *Chem. Rev.* **2016**, *116*, 2886 – 2936; b) W. T. Lee, S. B. Muñoz, D. A. Dickie, J. M. Smith, *Angew. Chem. Int. Ed.* **2014**, *53*, 9856 – 9859; *Angew. Chem.* **2014**, *126*, 10014 – 10017; c) Y. Gao, R. H. Crabtree, G. W. Brudvig, *Inorg. Chem.* **2012**, *51*, 4043 – 4050; d) S. Kal, L. Ayensu-Mensah, P. H. Dinolfo, *Inorg. Chim. Acta* **2014**, *423*, 201 – 206.

[12] G. Maayan, N. Gluz, G. Christou, *Nat. Catal.* **2018**, *1*, 48 – 54.

[13] M. Soler, W. Wernsdorfer, Z. Sun, J. C. Huffman, D. N. Hendrickson, G. Christou, *Chem. Commun.* **2003**, 2672 – 2673.

[14] a) R. Sessoli, H.-L. Tsai, A. R. Schake, S. Wang, J. B. Vincent, K. Folting, D. Gatteschi, G. Christou, D. N. Hendrickson, *J. Am. Chem. Soc.* **1993**, *115*, 1804 – 1816; b) R. Bagai, G. Christou, *Chem. Soc. Rev.* **2009**, *38*, 1011 – 1026.

[15] a) H. A. Chu, H. Sackett, G. T. Babcock, *Biochemistry* **2000**, *39*, 14371 – 14376; b) H. A. Chu, W. Hillier, N. A. Law, G. T. Babcock, *Biochim. Biophys. Acta Bioenerg.* **2001**, *1503*, 69 – 82; c) N. Gluz, G. Maayan, *J. Coord. Chem.* **2018**, *71*, 1971 – 1984.

[16] S. Verma, A. Verma, A. K. Srivastava, A. Gupta, S. P. Singh, P. Singh, *Mater. Chem. Phys.* **2016**, *177*, 140 – 146.

[17] H. Schiller, H. Dau, *J. Photochem. Photobiol. B* **2000**, *55*, 138 – 144.

[18] a) L. P. Souza, F. Calegari, A. J. G. Zarbin, L. H. Marcolino-Júnior, M. F. Bergamini, *J. Agric. Food Chem.* **2011**, *59*, 7620 – 7625; b) J. H. Luo, B. L. Li, N. B. Li, H. Q. Luo, *Sens. Actuators B*

2013, *186*, 84 – 89; c) D. M. Stanković, M. Ognjanović, M. Fabian, L. Švorc, J. F. M. L. Mariano, B. Antić, *Anal. Biochem.* **2017**, *539*, 104 – 112; d) I. Ali, S. Omanovic, *Int. J. Electrochem. Sci.* **2013**, *8*, 4283 – 4304.

[19] a) H. Lund, O. Hammerich, *Organic Electrochemistry*, 4th ed., Dekker, New York, **2001**; b) C. W. Lange, C. G. Pierpont, *Inorg. Chim. Acta* **1997**, *263*, 219 – 224; c) C. G. Pierpont, R. M. Buchanan, *Coord. Chem. Rev.* **1981**, *38*, 45 – 87.

[20] N. Kaeffer, A. Morozan, J. Fize, E. Martinez, L. Guetaz, V. Artero, *ACS Catal.* **2016**, *6*, 3727 – 3737.

[21] a) E. S. Rountree, B. D. McCarthy, T. T. Eisenhart, J. L. Dempsey, *Inorg. Chem.* **2014**, *53*, 9983 – 10002; b) C. Costentin, S. Drouet, M. Robert, J. M. Saveant, *J. Am. Chem. Soc.* **2012**, *134*, 11235 – 11242.

[22] J. M. Savéant, *Elements of Molecular and Biomolecular Electrochemistry: An Electrochemical Approach to Electron Transfer Chemistry*, Wiley, New York, **2000**.

[23] a) C. Costentin, G. Passard, J.-M. Savéant, *J. Am. Chem. Soc.* **2015**, *137*, 5461 – 5467; b) A. J. Bard, L. R. Faulkner, *Electrochemical Methods: Fundamentals and Applications*, 2nd ed., Wiley, New York, **2000**.

[24] a) H. Dau, C. Limberg, T. Reier, M. Risch, S. Roggan, P. Strasser, *ChemCatChem* **2010**, *2*, 724 – 761; b) X. Sala, S. Maji, R. Bofill, J. García-Anton, L. Escriche, A. Llobet, *Acc. Chem. Res.* **2014**, *47*, 504 – 516; c) T. J. Meyer, M. V. Sheridan, B. D. Sherman, *Chem. Soc. Rev.* **2017**, *46*, 6148 – 6169.

[25] a) T. F. Hughes, R. A. Friesner, *J. Phys. Chem. B* **2011**, *115*, 9280 – 9289; b) S. Khan, K. R. Yang, M. Z. Ertem, V. S. Batista, G. W. Brudvig, *ACS Catal.* **2015**, *5*, 7104 – 7113; c) B. Rudshteyn, K. J. Fisher, H. M. C. Lant, K. R. Yang, B. Q. Mercado, G. W. Brudvig, R. H. Crabtree, V. S. Batista, *ACS Catal.* **2018**, *8*, 7952 – 7960.

[26] Y. Yan, J. S. Lee, D. A. Ruddy, *Inorg. Chem.* **2015**, *54*, 4550 – 4555.

Manuscript received: December 6, 2018
Revised manuscript received: January 3, 2019
Version of record online: January 29, 2019

